PERGAMON

Atmospheric Environment 35 (2001) 3229–3240

ATMOSPHERIC ENVIRONMENT

www.elsevier.com/locate/atmosenv

Real-time measurements of the chemical composition of size-resolved particles during a Santa Ana wind episode, California USA

Sergio A. Guazzotti, Jeffery R. Whiteaker, David Suess, Keith R. Coffee, Kimberly A. Prather*

Department of Chemistry, University of California, Riverside, CA 92521, USA

Received 3 August 2000; accepted 5 February 2001

Abstract

Size-resolved particle composition, mass and number concentrations, aerosol scattering coefficients, and prevailing meteorological conditions were measured at the Ellen Browning Scripps Memorial Pier located in La Jolla, California on 15 December 1998. Aerosol particles were sampled using a field transportable aerosol time-of-flight mass spectrometer, allowing for the continuous detection and characterization of single particles from a polydisperse sample. An extensive and rapid change in the chemical composition of aerosol particles with aerodynamic diameters between 1.0 and 2.5 μm has been observed during the onset of a Santa Ana Winds condition. Coincident with the observed change in meteorological conditions, a substantial decrease in sea salt particles corresponds to an increase in dust and carbon-containing particles. This paper examines observations of the rapid changes occurring in the chemical composition of single aerosol particles and demonstrates the new types of information that can be obtained by measuring single particle size and composition with high temporal resolution. © 2001 Published by Elsevier Science Ltd.

Keywords: Aerosol composition; Sea salt; Single particle analysis; Coastal aerosol; Dust

1. Introduction

Changes in the chemical composition of particles present in the marine atmosphere lead to changes in the refractive index, therefore affecting visibility and the radiation balance. Aerosol particle composition can play a significant role in a number of areas ranging from regulating climate (e.g. Charlson et al., 1987) to affecting human health (Vedal, 1997; Pope et al., 1991). Also, micrometer sized particles may act as effective agents in the nucleation of cloud water droplets. The sources of fine particles in the marine atmosphere remain poorly defined although homogeneous gas-to-particle formation has been observed and suggested as a possible source (Allen et al., 1999; Hoppel et al., 1994; Ayers and Gras, 1991; Hegg et al., 1991). In a marine environment, particles may also be generated by physical means during bubble-bursting occurring on the ocean surface (Despiau et al., 1996, Resch and Afeti, 1991; Cipriano et al., 1983). It has been estimated that as much as one third of the natural flux of aerosols to the atmosphere is of marine origin (Andreae, 1995; Jaenicke, 1984; Prospero et al., 1983). Also, transport of continental aerosols over oceanic regions has been reported even for remote locations far from identifiable sources (Hoppel et al., 1990; Satheesh et al., 1998; Prospero, 1979).

This study was carried out on 15 December 1998 at the Ellen Browning Scripps Memorial Pier (32°52′N, 117°15′W) located in La Jolla, California, (approximately 15 km to the North of San Diego) during the

*Corresponding author. Fax: +1-909-787-4713.
E-mail address: prather@citrus.ucr.edu (K.A. Prather).

1352-2310/01/$ - see front matter © 2001 Published by Elsevier Science Ltd.
PII: S1352-2310(01)00140-6

onset of a meteorological condition known as the Santa Ana Winds. This condition occurs mainly in the fall and wintertime in southern California, and gets its name from the Santa Ana Canyon through which it passes. Santa Ana Winds develop in the Sierra Mountain range and are forced downward into the Santa Ana Valley by high pressure from the north. Cool air from the mountain sinks into the valley and becomes compressed by higher pressures. This compression forces the air temperature to rise, warming the valley. The warming air usually becomes very dry with winds generally exceeding 8 m/s. These winds are rarely observed during the summer season. A discussion is presented on the relatively rapid changes observed in the chemical composition of the individual particles detected at the pier induced by the Santa Ana Winds.

2. Experimental details

Several different instruments were used in the study. An optical particle counter (OPC) from Particle Measuring Systems, Inc. was used to evaluate particle number concentrations in the different size bins provided by the instrument (from 0.1 to larger than 2.0 μm) and allows for comparison of number counts as a function of size with the aerosol time-of-flight mass spectrometer (ATOFMS). The tapered element oscillating microbalance (TEOM) from Rupprecht and Patashnick Co. Inc. is used to evaluate particle mass concentration for those particles with aerodynamic diameter smaller than 2.5 μm. The integrating nephelometer from Radiance Research allows determination of the aerosol scattering coefficient. The ATOFMS is used to evaluate the size and chemical composition of single particles detected during the study. All instruments were located at the end of the Ellen Browning Scripps Memorial Pier, approximately 300 m of the coast and 14 m above sea level outside under a canopy. No external sampling lines were used.

As described in previous publications (Gard et al., 1997, 1998; Noble and Prather, 1996; Silva and Prather, 1997), ATOFMS allows for the characterization of the aerodynamic diameter and chemical composition of single particles from a polydisperse aerosol in real-time. Details on the function of the transportable ATOFMS developed at the University of California, Riverside are described elsewhere (Gard et al., 1997). Briefly, particles are sampled from atmospheric pressure through a converging nozzle into a first region maintained at approximately 3 Torr. Due to this pressure differential, the gas undergoes a supersonic expansion and smaller particles are accelerated to higher terminal velocities than larger particles. After this first stage, the aerosol beam passes through two stages of differential pumping separated by skimmers. Upon traveling through these regions, some particles get pumped away and never reach the analysis region. Particles with smaller aerodynamic diameters diverge more than those with larger aerodynamic diameter. This factor contributes to differences in transmission efficiency for different particle sizes into the instrument. To compensate for this transmission efficiency, particle number concentration data obtained with an optical particle counter are compared with those obtained with the transportable ATOFMS at all times. The collimated particle beam then enters the light scattering region where the transit times for particles traveling between two continuous wave lasers, which are a known distance apart, are measured.

In order to obtain the corresponding particle aerodynamic diameter from the measured transit time between the two continuous wave lasers, the transportable ATOFMS is calibrated using polystyrene latex spheres (PSL, Interfacial Dynamics Corporation) of known size. Polystyrene latex spheres are suspended in water and atomized using a collison atomizer and then dried using two 30-cm diffusion dryers filled with silica gel. PSL particles with aerodynamic diameter of 0.3, 0.53, 0.91, 1.5, 2.0 and 2.4 μm were used for calibration during this study. For particles with aerodynamic diameter larger than 0.5 μm (which represents the relevant size range in this paper), the calibration curve can be fit to a linear equation using the least square method with a coefficient of regression (R^2) of 0.98. Each point in the size calibration curve represents the average velocity for at least 1000 particles detected in the ATOFMS. After being sized, the particles travel to the ion source region of a dual ion time-of-flight mass spectrometer. A Nd : YAG laser with a 266-nm pulsed output is used to desorb and ionize molecules from the sized particles.

3. Results and discussion

In the following sections, results derived from data collected with the different instruments employed during this field study are presented.

3.1. Prevailing meteorological conditions, Santa Ana Winds

In Fig. 1, meteorological conditions recorded at the Scripps Institution of Oceanography, Ellen Browning Scripps Memorial Pier site on 15 December 1998 are presented. Data corresponding to wind speed, wind direction, relative humidity and temperature were obtained at 5-min intervals. Meteorological information was obtained from the on-line Scripps Institution of

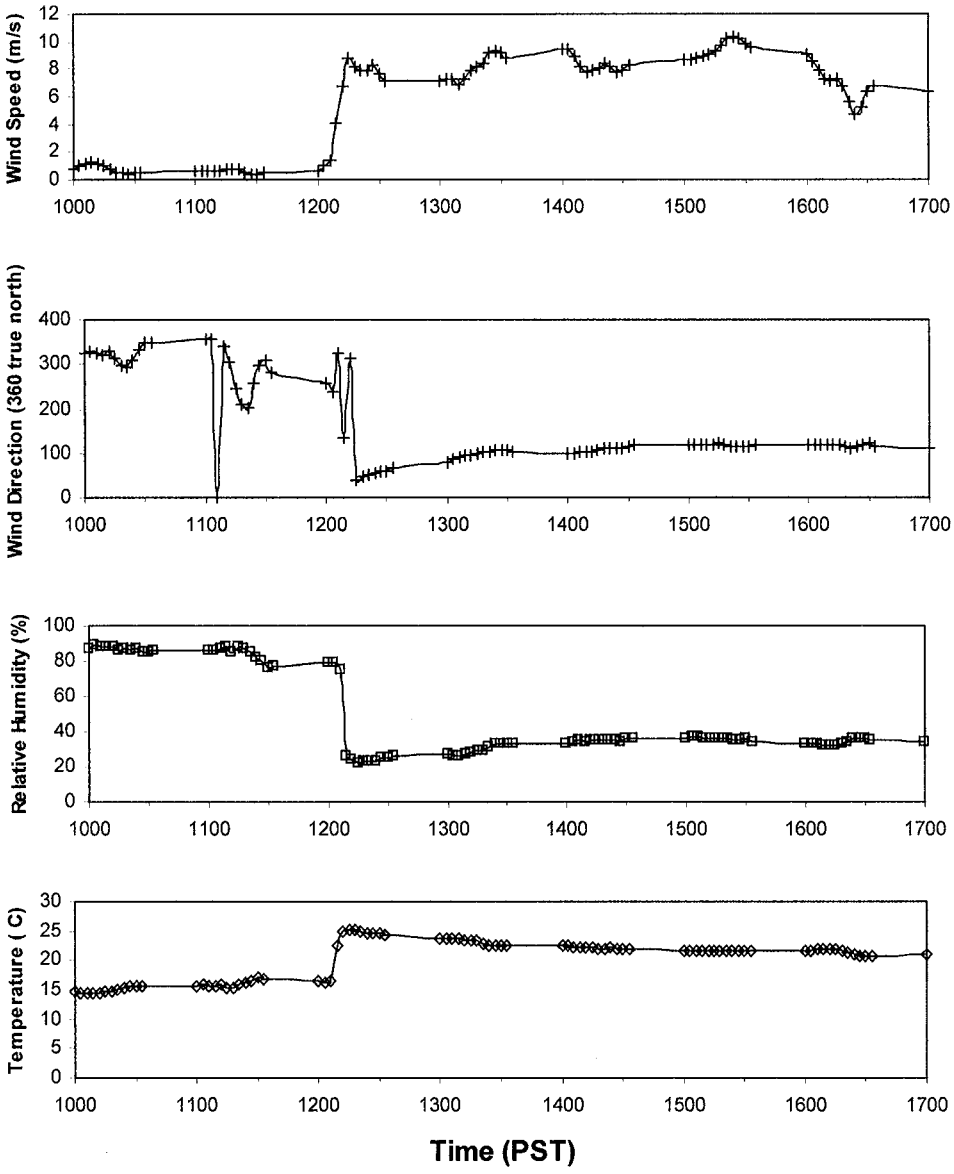

Fig. 1. Meteorological conditions, including wind speed, wind direction, relative humidity and temperature, observed at the Scripps Institution of Oceanography, Ellen Browning Scripps Memorial Pier on 15 December 1998.

Oceanography database. As shown in Fig. 1, there is a clear change in meteorological conditions taking place at 12:15 Pacific Standard Time (PST). At that time, wind speed increased from an approximate average of 1 m/s to as much as 9 m/s while a 10° increase in temperature and a 60% decrease in relative humidity were observed. Furthermore, the wind direction shifted from mostly north, northwest to east. These changes in meteorological conditions are associated with the presence of the Santa Ana Winds in Southern California, which have dry and warm characteristics.

3.2. Particle number concentration

Particle number concentrations, obtained with the OPC, for particles in the size ranges 0.2–1.0 μm, 1.0–2.0 μm, and larger than 2.0 μm are presented in Fig. 2. As shown in Fig. 2a, particle number concentrations for those particles with optical diameters between 1.0 and 2.0 μm show a relative increase starting at approximately 12:20 PST and a subsequent decrease at approximately 12:45 PST. For particles with optical diameters larger than 2.0 μm, particle number concentrations show an

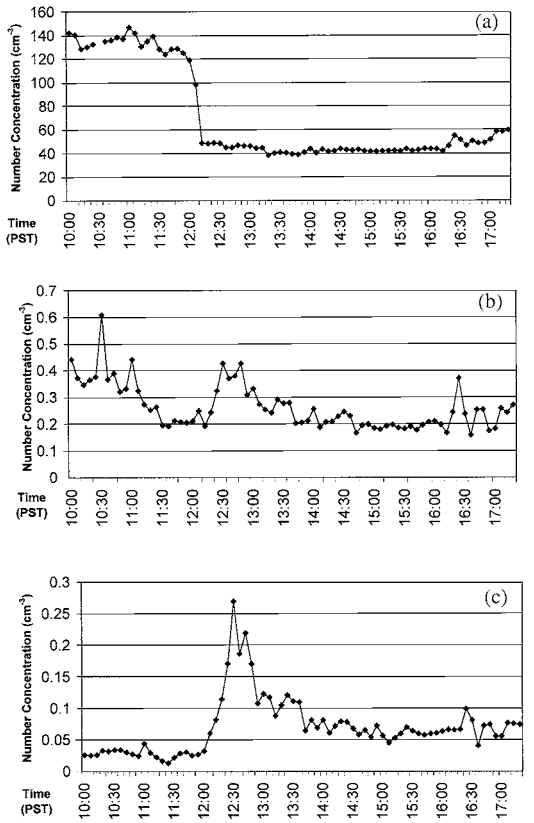

Fig. 2. Particle number concentration, as measured with an optical particle counter, on 15 December 1998 for particles with diameters (a) between 0.2 and 1.0 μm, (b) between 1.0 and 2.0 μm and (c) larger than 2.0 μm.

increase starting at approximately 12:00 PST, reaching a maximum value of 0.28 cm^{-3} at 12:20 PST. Following this period, a progressive decrease in particle concentration was observed at approximately 12:50 PST, with an average value of 0.05 cm^{-3} in the afternoon (Fig. 2b). For particles with diameter smaller than 1.0 μm, number concentrations decreased substantially starting at approximately 12:20 PST (Fig. 2c).

3.3. Particle mass concentration

Particle mass concentrations for particles with aerodynamic diameter smaller than 2.5 μm were evaluated with a tapered element oscillating microbalance (TEOM). Concentration values (30 min averages) obtained with the TEOM are presented in Fig. 3. Particle mass concentration ($PM_{2.5}$) decreased to an average value of approximately 7 $\mu g/m^3$ after 12:15 PST, from a maximum value of more than 20 $\mu g/m^3$ earlier in the morning. This decrease in particle mass concentration correlates with the observed decrease in particle number concentration and also with the change in meteorological conditions.

3.4. Aerosol scattering coefficient

Aerosol scattering coefficients were measured using a single wavelength (530 nm) integrating nephelometer (Radiance Research). The values observed during this study are shown in Fig. 4. As shown, there is a substantial decrease in the aerosol scattering coefficient value from approximately $6.95 \times 10^{-4}\,m^{-1}$ in the morning to approximately $6.60 \times 10^{-4}\,m^{-1}$ in the early afternoon. This change takes place over a short period of time at approximately 12:15 PST. Such a change in this parameter can be associated with a change in the aerosol concentration and/or chemical composition, and corresponds to an increase in visibility of approximately 5%. As mentioned previously, particle number concentrations for particles with diameters between 0.2 and 1.0 μm showed a decrease during the afternoon at approximately the same time the measured aerosol scattering coefficient values started to decrease. Fig. 4 also shows that, starting at approximately 15:30 PST, the values of aerosol scattering coefficients started to increase again, but never reached values as high as those recorded on the morning of 15 December 1998.

3.5. Particle size distribution

Size histograms are presented in Fig. 5 representing the raw number of particles in each size bin detected with the transportable ATOFMS in 30-min intervals. The histograms shown in the figure are not corrected for instrumental transmission efficiency since relative differences between different time periods are more obvious with uncorrected ATOFMS data. As illustrated in the corresponding figure, for all of the time periods presented, the majority of the particles detected in the instrument have aerodynamic diameters larger than 0.75 μm. Smaller particles were detected during the study however with 30 min time resolution, the number of counts were relatively small compared to coarse mode particles. When the different size histograms are compared, a decrease in the total number of particles detected is noticeable as the day progresses (indicated by the area under each of the curves). This observation is consistent with data from the TEOM and the OPC, where decreases in particle mass and number concentration were detected over the same time period.

Also as shown in Fig. 5, a relative change in the size distribution starting at 13:30 PST occurred, shifting slightly towards smaller particle sizes in the corresponding size histograms.

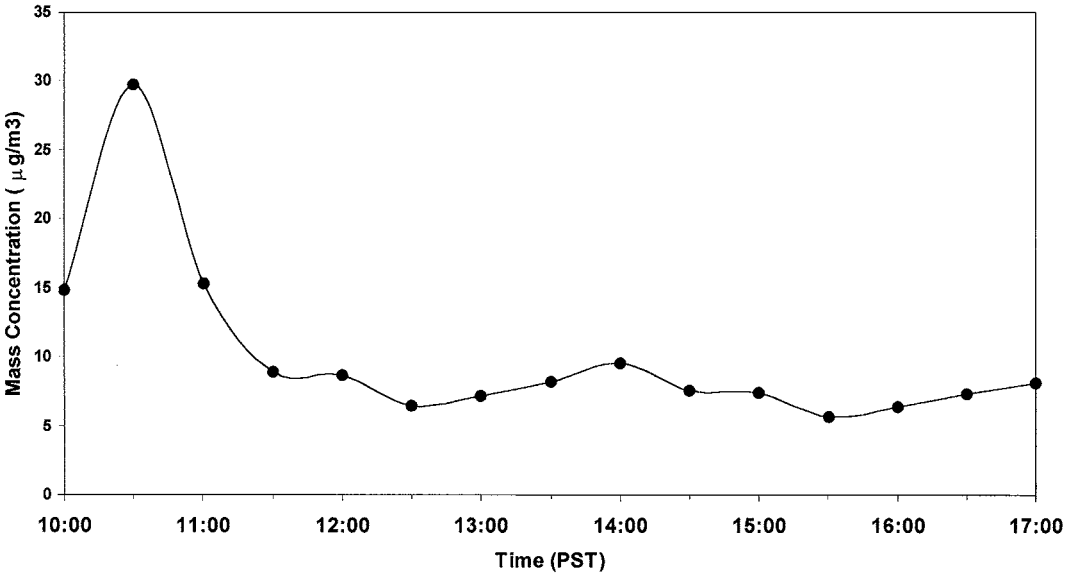

Fig. 3. Particle mass concentrations ($\mu g/m^3$) as measured with the tapered element oscillating microbalance (TEOM) described in the text on 15 December 1998. Each point in the plot represents a 30-min average concentration for particles with aerodynamic diameter smaller than 2.5 μm, with the value corresponding to the beginning of the sampling interval.

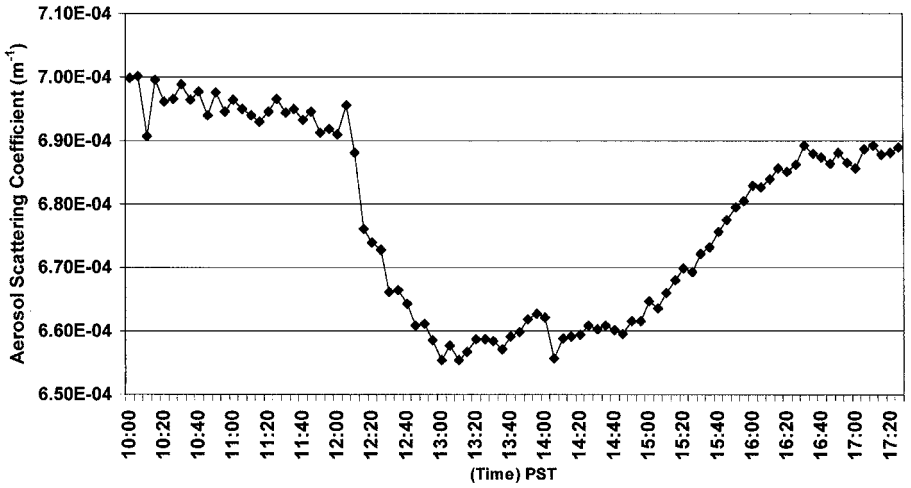

Fig. 4. Temporal variation of the aerosol scattering coefficient (b_{scat}) on 15 December 1998. Data obtained with the single wavelength (530 nm) integrating nephelometer described in the text.

3.6. Aerosol chemical composition

Aerosol chemical composition can be determined with the transportable ATOFMS from the positive and negative ion mass spectra for single particles. Detected particles are classified into exclusive chemical categories from the mass spectral information. Once each detected particle is classified into a category, the aerosol chemical composition is evaluated as the percentage of particles classified in each category for a corresponding size range. For the purpose of this paper, only particles with aerodynamic diameter between 1.0 and 2.5 μm are considered in this classification, since a substantial fraction of the particles observed with the ATOFMS during this study occurred in this size range.

In a first general scheme, particles can be classified into four chemically distinct categories: sea salt, dust, elemental carbon, and carbon-containing, with the first

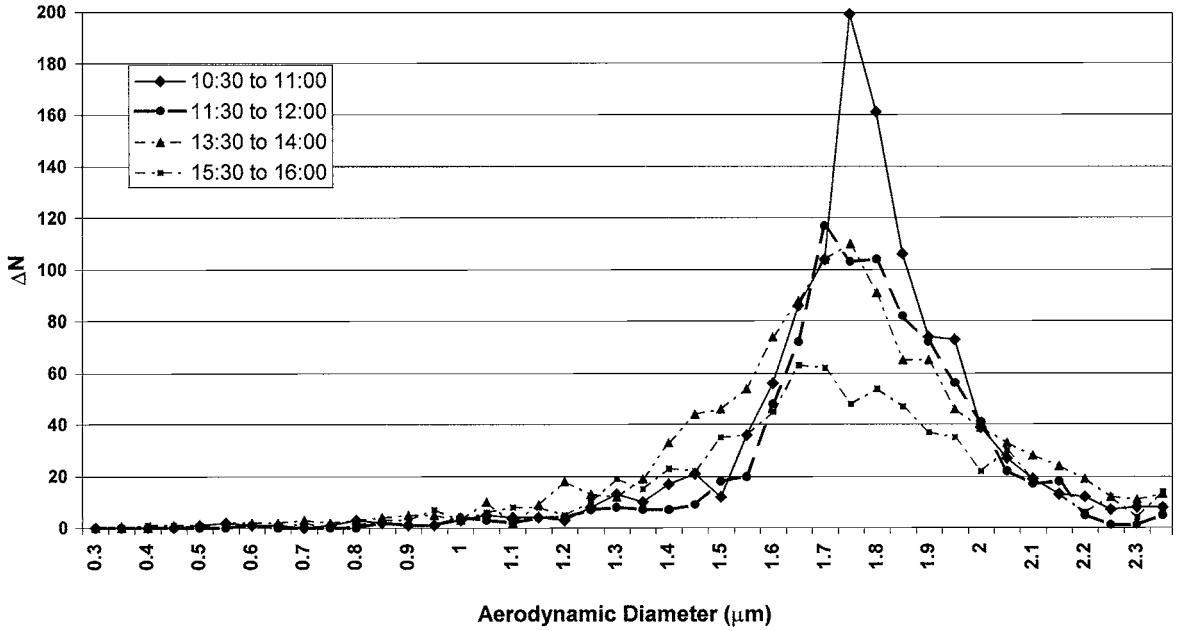

Fig. 5. Size histograms of particles sampled with a transportable ATOFMS on 15 December 1998. Four 30-min intervals are shown for comparison.

two classes representing more than 70% of the particles with aerodynamic diameter between 1.0 and 2.5 μm at all times. In Fig. 6a and b, laser desorption/ionization (LDI) mass spectra representative of a single particle classified as sea salt are presented. The positive ion mass spectrum shown in Fig. 6a corresponds to a particle with an aerodynamic diameter of 1.9 μm that was detected at 10:19 PST on 15 December 1998. The main features of the positive ion mass spectrum for this sea salt particle are the peaks at mass-to-charge ratios 23, 46, 62, 63, 81 and 83 that can be assigned to Na^+, Na_2^+, NaO^+, Na_2OH^+, $Na_2^{35}Cl^+$, $Na_2^{37}Cl^+$, respectively. Also peaks that correspond to Ca^+ and K^+ ions are evident at mass-to-charge ratios 40 and 39 and 41, respectively. The high intensity observed for the peak at mass-to-charge ratio 41 is most likely due to the formation of the $(Na(H_2O))^+$ ion cluster at high relative humidity. For the same sea salt particle, the negative ion mass spectrum is shown in Fig. 6b. The most noticeable features in the spectrum are the presence of peaks at mass-to-charge ratios −46, −62, −93, −95, and −97 that can be assigned to NO_2^-, NO_3^-, $Na^{35}Cl_2^-$, $(Na^{35}Cl^{37}Cl)^-$ and $Na^{37}Cl_2^-$, respectively. Peaks at mass-to-charge −16, −17, −35 and −37 are also typically observed in sea salt particles, and correspond to O^-, OH^-, $^{35}Cl^-$ and $^{37}Cl^-$ ions. The presence of nitrate on this sea salt particle indicates exposure to polluted air during the morning stagnant conditions.

The spectra presented in Fig. 6c and d are for a single particle classified as dust detected at 15:38 PST. This particle had an aerodynamic diameter of 1.7 μm. The main features in the positive ion mass-spectrum (Fig. 6c) are the peaks at mass-to-charge ratios 23, 27, 40 and 56 that can be assigned to Na^+, Al^+, Ca^+ and CaO^+, respectively. In the negative ion mass spectrum (Fig. 6d), peaks assigned to $^{16}O^-$, $^{17}OH^-$, $^{59}(AlO_2)^-$ are observed.

Ions commonly observed in the mass spectra of particles classified as carbon-containing are those associated with carbon–hydrogen clusters including $^{12}C^+$, $^{15}(CH_3^+)$, $^{24}(C_2^+)$, $^{27}(C_2H_3^+)$, $^{36}(C_3^+)$, $^{37}(C_3H^+)$ and others ion peaks associated with the hydrocarbon envelopes ($C_nH_m^+$). Some common negative ions found in these particles are $^{12}C^-$, $^{24}(C_2^-)$, $^{25}(C_2H^-)$, $^{36}(C_3^-)$ and $^{48}(C_4^-)$. Some of these particles also show peaks due to $^{39}K^+$ (associated with combustion sources) and $^{97}(HSO_4^-)$.

In the case of particles classified as elemental carbon (EC), it is possible to observe in the positive ion mass spectra the presence of carbon ion clusters that extend to higher mass-to-charge ratios than in the case of carbon-containing particles. Usually the intensity of the singly protonated clusters (C_nH^+) present in the EC spectra are much lower than in the case of carbon-containing particles, and higher protonated clusters are usually missing in this particle class. In the negative ion mass spectra, a peak at mass-to-charge –72, assigned to (C_6^-), is usually observed. For some of these particles, $^{80}(SO_3^-)$ and $^{97}(HSO_4^-)$ ion clusters are detected in the corresponding negative ion mass spectra.

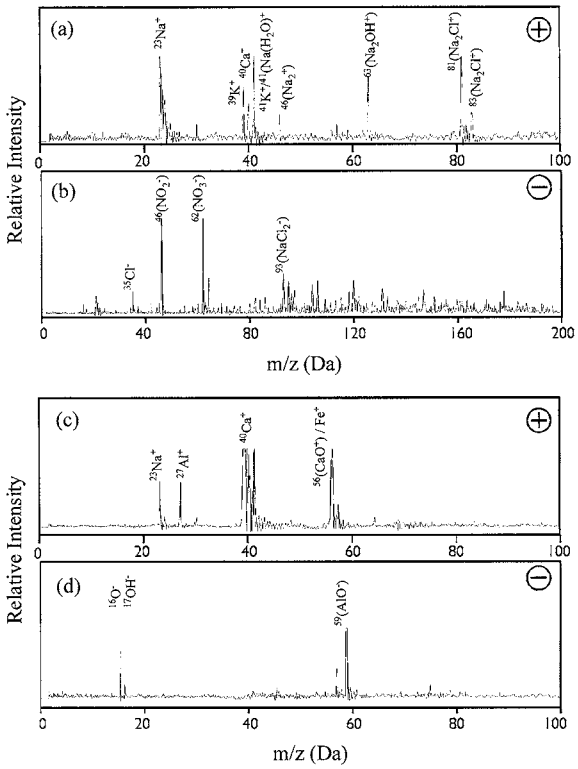

Fig. 6. Positive (a) and negative (b) ion mass spectra of a single sea salt particle with aerodynamic diameter of 1.9 μm detected at 10:19 PST on 15 December 1998. Positive (c) and negative (d) ion single particle mass spectra for a 1.7 μm dust particle detected at 15:35 PST on 15 December 1998. Peak identifications correspond to the most probable ions for the particular mass-to-charge ratio.

In order to evaluate changes in the aerosol chemical composition, eleven time periods, ten with 30-min resolution and one with 45-min resolution, are selected to classify the detected particles into one of the four general classes mentioned above. The results from the analysis are shown in Fig. 7a. In the figure, the percentages of particles classified into one of the four exclusive categories are shown for each of the described time periods. The number of particles in each class detected in the ATOFMS is corrected for transmission efficiency, using the OPC data, prior to the determination of percentages. The difference in observed aerosol chemical composition is more apparent with two contrasting time periods. The first selected period is from 10:15 to 12:15 PST and the second from 12:15 to 16:00 PST. These are selected to represent periods before and after the onset of the Santa Ana Winds in the study location. In the 10:15 to 12:15 PST and 12:15 to 16:00 PST time periods, 1844 and 1709 particles were chemically analyzed, respectively. In Fig. 7b, the chemical compositions of the particles present during the two time periods are compared. As shown in the figure, there is a large increase, from 3.4% to 37.5%, in the percentage of particles classified as mineral dust from the morning to the afternoon on 15 December 1998. A substantial decrease in sea salt particles, from 93.6% to 31%, is observed when the two time periods are compared. Also, increases in the contributions from particles classified as elemental carbon (from 0% to 4.3%) and carbon-containing (from 2% to 9%) are observed for the afternoon period. Before 12:15 PST, the aerosol chemical composition was typical for a marine environment in the southern California region and similar to previous results obtained earlier the same year at that Scripps Institution of Oceanography Pier with an identical instrumental set-up. After 12:15 PST, the onset of the Santa Ana Winds transported a continental air mass to the sampling site that presented more inland characteristics as indicated by a higher percentage of dust and organic-related particles.

Additional peaks in the mass spectra obtained for the particles allow further classifications to be carried out. For this study, differences in composition from particles classified as sea salt permit this class to be subdivided into eight categories: (a) unreacted sea salt particles, (b) reacted sea salt particles with nitrates, (c) sea salt particles with organic matter, (d) reacted sea salt

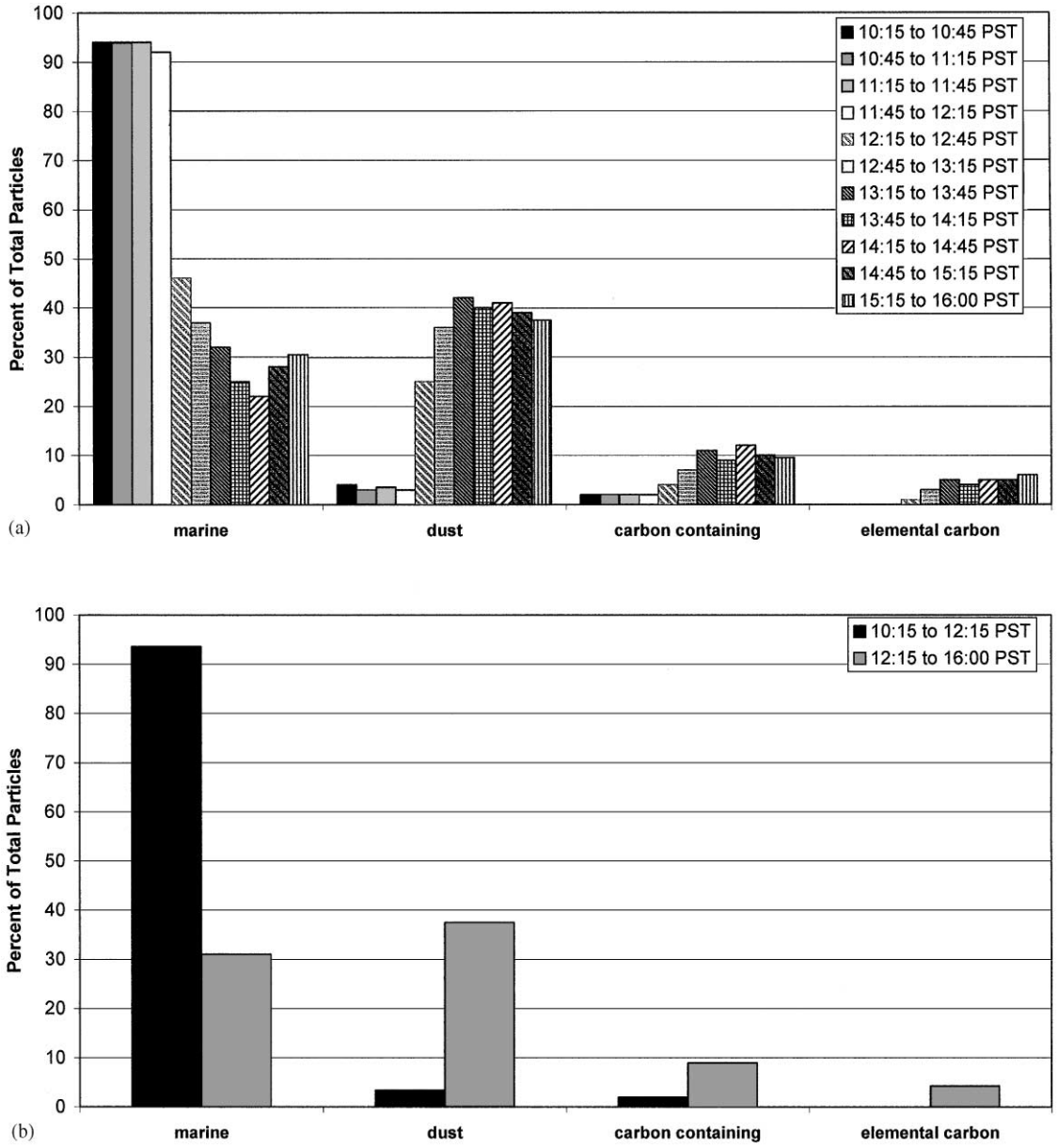

Fig. 7. Aerosol chemical composition as determined from the single particle mass spectra collected with a transportable ATOFMS. The y-axis represents the percentage of particles classified into one of the four specified classes based on the mass spectral characteristics. In (a), eleven time periods are selected for the analysis. In (b), the results are grouped into two time periods.

particles with nss (non sea salt) sulfates, (e) sea salt particles with organic matter and nitrates, (f) sea salt particles with organic matter and nss sulfates (g) sea salt particles with nitrates and nss sulfates, and (h) sea salt particles with organic matter, nitrates, and nss sulfates.

With the exception of the unreacted sea salt class, all other classes mentioned above describe aged and/or reacted sea salt particles. These particles are typically aged by exposure to different emissions such as sulfuric acid, inorganic sulfates, organic sulfates, nitric acid, nitrogen oxide species, and organic compounds (Song and Carmichael, 1999). The ability to differentiate between these types of particles is relevant because the hygroscopic behavior of the aerosol particles will be affected by the presence of internally mixed components and also because sulfate associated aerosols have the potential to modify the radiation budget of the atmosphere (e.g. Langman et al. 1998).

In the case of particles classified as reacted sea salt with nitrates, chlorine displacement from the particle, with the subsequent formation of sodium nitrate in the particle phase, is indicated by the presence of $^{108}(Na_2NO_3^+)$ (Gard et al., 1998 and references therein). Reacted sea salt particles with nss sulfate show a peak in their mass spectra at mass-to-charge 165, $(Na_3SO_4^+)$, with relative intensities higher than 1%. This threshold, determined in previous lab and field experiments, discriminates between natural levels of sulfate in sea water and nss sulfate. In sea salt particles, the sulfate could result from uptake by condensation of sulfuric acid (or organic sulfates) from the gas phase and/or by conversion of dissolved SO_2 (Kerminen et al., 1998; Clegg and Toumi, 1998). Sea salt particles with organic matter contain additional mass spectral peaks due to $^{12}C^+$ and $^{12}C^-$. The presence of organic matter in these particles could also result from heterogeneous reactions

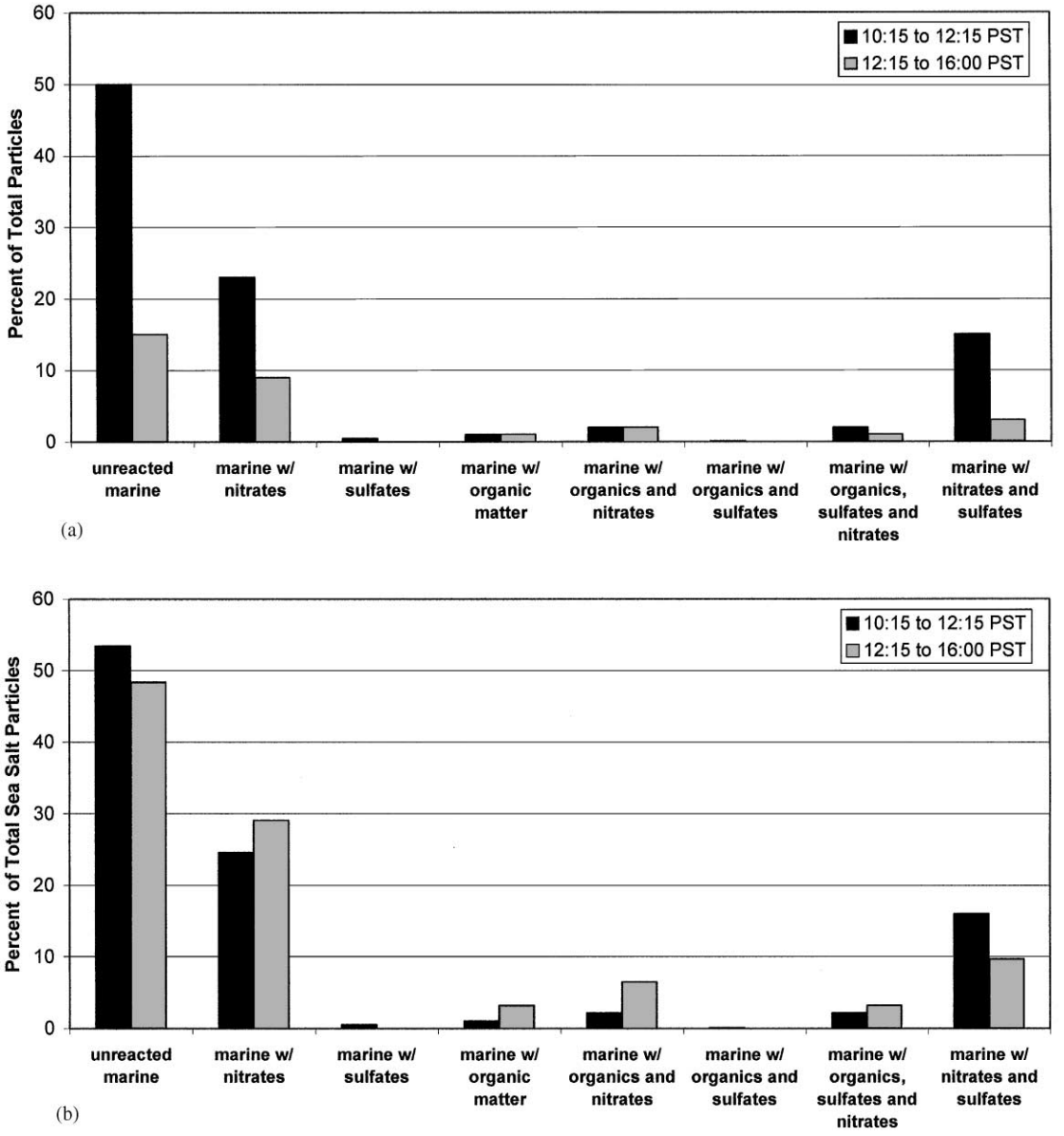

Fig. 8. Aerosol chemical composition as determined from ATOFMS single particle analysis for two time periods before and after the onset of the Santa Ana Wind condition, as specified in the text. In (a), eight sea salt-related particle classes are shown, with the *y*-axis representing the percentage of particles that were classified into one of the specified classes based on the mass spectral characteristics. In (b), eight sea salt-related classes are shown with the *y*-axis representing the contribution of each class with respect to the total number of sea salt particles during each interval.

or condensation of organic vapors (Kerminen et al., 1998; Tseng et al., 1992).

The other particle classes (sea salt particles with organic matter and nitrates; sea salt particles with organic matter and nss sulfates; sea salt particles with nitrates and nss sulfates; sea salt particles with organic matter, nitrates, and nss sulfates) have peaks in their spectra consisting of combinations of the peaks described above for the more simple classes. For example, sea salt particles with organic matter and nitrates show in their mass spectra additional peaks due to $^{12}C^+$ and $^{12}C^-$, as well as the presence of $^{108}(Na_2NO_3^+)$. In Fig. 8a, the contributions from these sea salt-related classes to the aerosol chemical composition are shown for the same two time periods used in the initial general classification. As shown in the figure, contributions from all classes are higher (or equal in the case of sea salt with organic matter and sea salt with organic matter and nitrates) for the earlier time period before the onset of the Santa Ana Winds. Contributions from unreacted sea salt, reacted sea salt with nitrates, and reacted sea salt with nitrates and sulfates particle classes are higher than those for the remaining sea salt-related classes in both time periods. Unreacted sea salt particles showed a decrease in their contribution from 50% to 15% from the morning to the afternoon, whereas reacted sea salt particles with nitrates decreased from 23% to 9%.

When the contribution from reacted sea salt particles with nitrates is compared with the corresponding contribution from unreacted sea salt, it is found that the ratio between the former and the latter classes is 0.46 for the morning time period and 0.60 for the afternoon period. The higher ratio found for the 12:15–16:00 PST period could indicate that the air mass arriving at the site in the afternoon existed for a longer time over land where pollutants exist, allowing reactions to take place and/or formation of nitric acid from emissions (Gard et al., 1998). This is shown in Fig. 8b where the contributions to the aerosol chemical composition from sea salt related classes are shown with respect to the total number of sea salt particles in each time period. Higher contributions form sea salt particles with organics are observed in the afternoon period (as shown in Fig. 8b), most likely as a consequence of an increase in organic gases in the polluted air condensing on the sea salt particles. No substantial changes in the contribution of sea salt particles with sulfates are detected for the afternoon period probably due to the fact that no major sources of SO_2 were encountered by the air mass arriving to the sampling site. Also, as a consequence of this change in aerosol chemical composition, the refractive properties of the particles being detected in the ATOFMS changed from the morning to the afternoon affecting the radiative properties of the atmospheric aerosol. The aerosol characteristics changed from those characteristics of a marine environment (in the morning) to those showing inland influences (in the afternoon). As mentioned previously, the aerosol scattering coefficient showed a decrease from the morning to the afternoon. This change could therefore be correlated not only with the decrease in particle number concentration but also with the described variation in the aerosol chemical composition.

4. Conclusions

Using a transportable ATOFMS changes in the aerosol chemical composition with the onset of a Santa Ana Winds condition were detected and evaluated. When the wind direction changed, a substantial decrease in the percentage of particles classified as sea salt corresponded with an increase in the number of particles classified as dust and carbon-containing. This shows the significant contrast between particles in an air mass with marine characteristics and those in an air mass with inland attributes, a change that can occur in a very short time period.

In order to assess the effect of aerosols on visibility, radiation balance, and human health, it is of extreme importance to be able to follow variations in single particle size and chemical composition characteristics with time. In this study, ATOFMS single particle analysis allowed for the detection of substantial changes in aerosol composition that took place over a short time frame (approximately 30 min) with high temporal resolution. The longer sampling intervals required for most off-line aerosol analysis techniques would have precluded the observation of such rapid changes in aerosol properties. Also, with off-line techniques, it would be difficult and impossible to choose a priori two sampling events that capture the rapid change in the aerosol that occurred during this event. Semi-continuous methods used for monitoring aerosol chemical composition, such as thermal analysis, automated ion chromatography and flash-vaporization have the advantage over traditional off-line techniques of presenting higher temporal resolutions, but they only allow detection of certain specific species present in the aerosol particles at any one time (such as inorganic ions and particulate carbon) (e.g. Buhr et al., 1995; Karlsson et al., 1997; Poruthoor and Dasgupta, 1997; Simon and Dasgupta, 1995a, b; Slanina and Wyers, 1994; Stolzenburg and Hering, 2000; Turpin et al., 1990; Weber et al., 1999; Zellweger et al., 1999). ATOFMS analysis allows determination of variations in the combinations of present species, therefore allowing monitoring the evolution of particle types over time.

This study demonstrates the type of information that can be obtained by being able to follow transient events in aerosol chemical composition with the necessary temporal resolution. Information at this level of detail

can be used to refine atmospheric models used to predict the effects of aerosols on heterogeneous chemistry, global climate change, and visibility reduction.

Acknowledgements

The authors would like to express their gratitude to the people from the Scripps Institution of Oceanography, La Jolla for permission and accommodation in the use of the Ellen Browning Scripps Memorial Pier for this field experiment and for the assistance they have provided. We would like to extend special thanks to Dr. V. Ramanathan and Dr. Paul Crutzen for all their help throughout this project, as well as to the individuals who maintain and operate the meteorological equipment located on the Pier. The authors would also like to thank Dr. Antonio H. Miguel for the help he provided in editing this manuscript. This research was supported by the National Science Foundation via the Center for Clouds, Chemistry and Climate (Grants ATM9612887 and ATM9405024) and the U.S. Environmental Protection Agency (Award # R826240-01-0).

References

Allen, A.G., Grenfell, J.L., Harrison, R.M., James, J., Evans, M.J., 1999. Nanoparticle formation in marine airmasses: contrasting behaviour of the open ocean and coastal environments. Atmospheric Research 51, 1–14.

Andreae, M.O., 1995. In: Henderson-Sellers, A. (Ed.), Future Climates of the World: A Modeling Perspective. Elsevier, Amsterdam, New York, pp. 341–392.

Ayers, G.P., Gras, J.L., 1991. Seasonal relationship between cloud condensation nuclei and aerosol methanesulphonate in marine air. Nature 353, 834–835.

Buhr, S.M., Buhr, M.P., Fehsenfeld, F.C., Holloway, J.S., Karst, U., Norton, R.B., Parrish, D.D., Sievers, R.E., 1995. Development of a semi-continuous method for the measurement of nitric acid vapor and particulate nitrate and sulfate. Atmospheric Environment 29, 2609–2624.

Charlson, R.J., Lovelock, J.E., Andreae, M.O., Warren, S.G., 1987. Oceanic phytoplankton, atmospheric sulphur, cloud albedo and climate. Nature 326, 655–661.

Cipriano, R.J., Blanchard, D.C., Hogan, A.W., Lala, G.G., 1983. On the production of Aitken nuclei from breaking waves and their role in the atmosphere. Journal of the Atmospheric Sciences 40, 469–479.

Clegg, N.A., Toumi, R., 1998. Non-sea-salt-sulphate formation in sea-salt aerosol. Journal of Geophysical Research—Atmospheres 103, 31095–31102.

Despiau, S., Cougnenc, S., Resch, F., 1996. Concentrations and size distributions of aerosol particles in coastal zone. Journal of Aerosol Science 27, 403–415.

Gard, E.E., Kleeman, M.J., Gross, D.S., Hughes, L.S., Allen, J.O., Morrical, B.D., Fergenson, D.P., Dienes, T., Galli, M.E., Johnson, R.J., Cass, G.R., Prather, K.A., 1998. Direct observation of heterogeneous chemistry in the atmosphere. Science 279, 1184–1187.

Gard, E., Mayer, J.E., Morrical, B.D., Dienes, T., Fergenson, D.P., Prather, K.A., 1997. Real-time analysis of individual atmospheric aerosol particles: design and performance of a portable ATOFMS. Analytical Chemistry 69, 4083–4091.

Hegg, D.A., Ferek, R.J., Hobbs, P.V., Radke, L.F., 1991. Dimethyl sulfide and cloud condensation nucleus correlations in the northeast Pacific Ocean. Journal of Geophysical Research—Atmospheres 96, 13189–13191.

Hoppel, W.A., Fitzgerald, J.W., Frick, G.M., Larson, R.E., Mack, E.J., 1990. Aerosol size distributions and optical properties found in the marine boundary layer over the Atlantic Ocean. Journal of Geophysical Research—Atmospheres 95, 3659–3686.

Hoppel, W.A., Frick, G.M., Fitzgerald, J., Larson, R.E., 1994. Marine boundary layer measurements of new particle formation and the effects nonprecipitating clouds have on aerosol size distribution. Journal of Geophysical Research—Atmospheres 99, 14443–14459.

Jaenicke, R., 1984. In: Gerber, H.E., Deepak, A., et al. (Eds.), Aerosols and their Climatic Effects. A. Deepak Pub., Hampton, Va, pp. 7–34.

Karlsson, A., Irgum, K., Hansson, H.C., 1997. Single-stage flowing liquid film impactor for continuous on-line particle analysis. Journal of Aerosol Science 28, 1539–1551.

Kerminen, V.M., Teinila, K., Hillamo, R., Pakkanen, T., 1998. Substitution of chloride in sea-salt particles by inorganic and organic anions. Journal of Aerosol Science 29, 929–942.

Langman, B., Herzog, M., Graf, H.F., 1998. Radiative forcing of climate by sulfate aerosols as determined by a regional circulation chemistry transport model. Atmospheric Environment 32, 2757–2768.

Noble, C.A., Prather, K.A., 1996. Real-time measurement of correlated size and composition profiles of individual atmospheric aerosol particles. Environmental Science and Technology 30, 2667–2680.

Pope, C.A., Dockery, D.W., Spengler, J.D., Raizenne, M.E., 1991. Respiratory health and PM10 pollution—a daily time series analysis. American Review of Respiratory Disease 144, 668–674.

Poruthoor, S.K., Dasgupta, P.K., 1997. An automated instrument for the measurement of atmospheric aerosol composition. American Laboratory 29, 51pp.

Prospero, J.M., 1979. Mineral and sea salt aerosol concentrations in various ocean regions. Journal of Geophysical Research 84, 725–731.

Prospero, J.M., Charlson, R.J., Mohnen, V., Jaenicke, R., Delany, A.C., Moyers, J., Zoller, W., Rahn, K., 1983. The atmospheric aerosol system: an overview. Reviews of Geophysics and Space Physics 21, 1607–1629.

Resch, F., Afeti, G., 1991. Film drop distributions from bubbles bursting in seawater. Journal of Geophysical Research—Oceans 96, 10681–10688.

Satheesh, S.K., Moorthy, K.K., Murthy, B.V., 1998. Spatial gradients in aerosol characteristics over the Arabian sea and Indian Ocean. Journal of Geophysical Research—Atmospheres 103, 26183–26192.

Silva, P.J., Prather, K.A., 1997. On-line characterization of individual particles from automobile emissions. Environmental Science and Technology 31, 3074–3080.

Simon, P.K., Dasgupta, P.K., 1995a. Continuous automated measurement of gaseous nitrous and nitric acids and particulate nitrite and nitrate. Environmental Science and Technology 29, 1534–1541.

Simon, P.K., Dasgupta, P.K., 1995b. Continuous automated measurement of the soluble fraction of atmospheric particulate matter. Analytical Chemistry 67, 71–78.

Slanina, J., Wyers, G.P., 1994. Monitoring of atmospheric components by automatic denuder systems. Fresenius Journal of Analytical Chemistry 350, 467–473.

Song, C.H., Carmichael, G.R., 1999. The aging process of naturally emitted aerosol (sea-salt and mineral aerosol) during long range transport. Atmospheric Environment 33, 2203–2218.

Stolzenburg, M.R., Hering, S.V., 2000. Method for the automated measurement of fine particle nitrate in the atmosphere. Environmental Science and Technology 34, 907–914.

Turpin, B.J., Cary, R.A., Huntzicker, J.J., 1990. An in situ, time-resolved analyzer for aerosol organic and elemental carbon. Aerosol Science and Technology 12, 161–171.

Vedal, S., 1997. Ambient particles and health: lines that divide. Journal of the Air and Waste Management Association 47, 551–581.

Weber, R.J., Orsini, D., Duan, Y., 1999. A new instrument for near-continuous measurements of ambient aerosol chemical composition. American Association for Aerosol Research, Tacoma, WA.

Zellweger, C., Ammann, M., Hofer, P., Baltensperger, U., 1999. NO_y speciation with a combined wet effluent diffusion denuder-aerosol collector coupled to ion chromatography. Atmospheric Environment 33, 1131–1140.